Liquid lens confocal microscopy with advanced signal processing for higher resolution 3D imaging

Riza, Nabeel, Sheikh, Mumtaz

Nabeel A. Riza, Mumtaz A. Sheikh, "Liquid lens confocal microscopy with advanced signal processing for higher resolution 3D imaging," Proc. SPIE 7258, Medical Imaging 2009: Physics of Medical Imaging, 725848 (13 March 2009); doi: 10.1117/12.811338

SPIE.

Event: SPIE Medical Imaging, 2009, Lake Buena Vista (Orlando Area), Florida, United States

Liquid Lens Confocal Microscopy with Advanced Signal Processing for Higher Resolution 3D Imaging

Nabeel A. Riza and Mumtaz A. Sheikh
Photonic Information Processing Systems Laboratory,
CREOL, The College of Optics,
University of Central Florida,
4000 Central Florida Boulevard, Orlando, Florida 32816-2700, USA.
Email: riza@creol.ucf.edu, Lab Web site: http://pips.creol.ucf.edu

ABSTRACT

The paper first highlights the use of multiple electronically controlled optical lenses, specifically, liquid lenses to realize an axial scanning confocal microscope with potentially less aberrations. Next, proposed is a signal processing method for realizing high resolution three dimensional (3-D) optical imaging using diffraction limited low resolution optical signals. Using axial shift-based signal processing via computer based computation algorithm, three sets of high resolution optical data is determined along the axial (or light beam propagation) direction using low resolution axial data. The three sets of low resolution data are generated by illuminating the 3-D object under observation along its three independent and orthogonal look directions (i.e., x, y, and z) or by physically rotating the object by 90 degrees and also flipping the object by 90 degrees. The three sets of high resolution axial data is combined using a unique mathematical function to interpolate a 3-D image of the test object that is of much higher resolution than the diffraction limited direct measurement 3-D resolution. Confocal microscopy or optical coherence tomography (OCT) are example methods to obtain the axial scan data sets. The proposed processing can be applied to any 3-D wave-based 3-D imager including ones using electromagnetic waves and sound (ultrasonic) waves. Initial computer simulations are described to test the robustness of the proposed high resolution signal processing method.

1. INTRODUCTION

There are numerous applications where 3-D imaging of objects is desirable. Applications include the electromagnetic (EM) spectrum to ultrasonic frequencies. Instruments for example include Radio Frequency (RF) radar, optical radar, X-ray imagers, optical microscopes, and ultrasound. In general, the wave properties of the probing signal in combination with the material properties of the test object limits the 3-D resolution of the imager. In classical wave optics (EM radiation), wave diffraction sets a limit on the smallest size the optical imager can see in the transverse direction, this limit called the Abbe limit given by $0.5\lambda/\text{N.A.}$, where N.A is the numerical aperture of the aperture times the refractive index n of the medium in which the object is observed. For a given microscope objective lens, $\text{N.A.} = n \sin\theta$, where θ is the maximum half angle that the lens can capture to pick up the highest spatial frequency in the object. In the axial direction, diffraction also plays its limiting role such as in confocal microscopes where the axial resolution (Full-Width-Half-Max: FWHM) can be typical given by $1.4n\lambda/(\text{N.A.})^2$. For example, with n=1 (air), N.A.=1.3, and red light with λ=633 nm, the transverse and FWHM axial resolution are 0.24 microns and 0.5 microns, respectively. In alternate OCT systems, the axial resolution is limited by the coherence length limit of the illuminating radiation, i.e., broader the EM bandwidth, the smaller the axial resolution. In effect, both axial and transverse resolution of optical imagers is on the order of the optical wavelength. It would be highly desirable if optical imagers could see in 3-D with resolution far better than the order of wavelength, perhaps, a 100 or 1000 times smaller than the wavelength. Ultimately, the voxel produced would be a high resolution voxel no longer limited in size by the classic diffraction or coherence limits.

Today, the Abbe resolution still holds strong in optical imagers/microscopes. Various approaches have been tried to improve the axial and transverse resolution of microscopes such as listed in [1-9]. One way to get better resolution is via image processing algorithms [10]. Images can get blurred due to fast motion of objects and/or because the image is out of focus because of imperfect imaging conditions. Image sharpening algorithms have been developed that can reduce the image blur or defocus giving higher resolution images. One such successful algorithm involves taking high resolution shifts of low resolution images and then Iterative Back-Projection (IBP) processing to generate the high resolution image

Medical Imaging 2009: Physics of Medical Imaging, edited by Ehsan Samei, Jiang Hsieh,
Proc. of SPIE Vol. 7258, 725848 · © 2009 SPIE
CCC code: 1605-7422/09/$18 · doi: 10.1117/12.811338

[11]. Such an iterative algorithm has been applied to produce higher resolution images such as in remote sensing [12] and 2-D and 3-D super-resolution on single shot Magnetic Resonance Imaging (MRI) [13]. Other image restoration algorithms have also been applied to 3-D optical microscopy to improve imaging resolution such as in [14] and [15]. Here, complete 2-D image slices are acquired for different finely tuned focus positions and then this image data is processed. Other successful image processing algorithms applied to high resolution imaging via use of shifted low resolution images include Maximum Likely-Hood Estimation (MLE) and Iterative Blind Deconvolution (IBD) [16, 17]. In these computer based algorithms, one uses the given (by theory) or acquired (by experiment) or estimated Point Spread Function for the imager along-with the high resolution shifted images to reconstruct the high resolution image or 3-D data. As an example, given a low resolution voxel size of X per side, a high resolution shift would be of X/(2N) implemented for both image directions and 2N x 2N images are acquired and then processed to finally give a high resolution image with a pixel size of X/N per side. In effect, using these computer algorithms as is done today, massive amount of data processing is required. As shown later, the proposed 3-D imaging scheme uses line or one dimensional (1-D) signal space data along the axial direction to produce the needed high resolution 1-D slices instead of the much larger image or two dimensional (2-D) signal space data acquired in the transverse direction suffering the Abbe limit. As such, must faster computation can be implemented by the proposed approach.

In addition, prior art shows that breaking the optical limits is not a repudiation of the laws of physics. Nature performs similar interpolation-like brain processing when human vernier acuity tasks are performed to give an order of magnitude better vision than the eye spatial sampling hardware (i.e., cone spacing) allows [18]. Analysis of this phenomenon with broadly tuned sensors yield very high spatial resolutions (error less than 10^{-4}) [19, 20]. This interpolation technique of reconstructing fine detail from coarse input sensors can also be utilized to enhance biological and artificial spectrum analyzers [21].

Proposed in the second part of this paper is an alternate signal processing method for realizing high resolution 3-D optical imaging using diffraction limited low resolution optical signals. Three sets of high resolution optical data is determined along the axial (or light beam propagation) direction. The three sets are generated by illuminating the 3-D object under observation along its three independent and orthogonal look directions (i.e., x, y, and z). Alternately, the object can be physically rotated by 90 degrees and also flipped by 90 degrees to get the required three sets of data that is diffraction limited in the transverse spatial direction but high resolution in the axial direction. Because the axial resolution is also limited by optical diffraction or temporal coherence effects, the directly measured axial resolution is also limited to a low spatial resolution signal. By taking many low resolution axial data, each for a small high resolution axial shift of the object under illumination (or shift of the optical beam axial minimum), a high resolution optical data signal for the axial direction of the object can be obtained after computer-based signal processing. The three sets of high resolution axial data (each low resolution in its given transverse direction) can be then combined using a special mathematical function to interpolate a 3-D image of the test object that is of much higher resolution than the diffraction limited direct measurement 3-D resolution. Confocal microscopy or optical coherence tomography (OCT) are example methods to obtain the axial scan data sets. The proposed processing can be applied to any 3-D wave-based 3-D imager including ones using electromagnetic waves and sound (ultrasonic) waves.

Recently we have demonstrated biological 3-D imaging of a blood vessel using an electronically controlled optical lens to accomplish no-moving parts depth section scanning in a modified commercial 3-D confocal microscope. Our study shows that the liquid crystal electronic lens-based 3-D views are limited by the aberrations in the liquid crystal lens device. The first part of this paper highlights the use of an alternative E-lens technology called liquid lens that is deployed as multiple E-lenses to realize an axial scanning confocal microscope with potentially less aberrations.

2. PROPOSED LIQUID LENS-BASED CONFOCAL MICROSCOPY SYSTEM

Earlier was proposed and demonstrated E-lens based confocal architectures [22, 24-27] to 3-D image a specimen. Fig. 1 shows a novel extension of the earlier work. In particular, proposed is a liquid lenses based minimal-moving parts confocal microscope system design. Like before, both the sample and the objective remain fixed while axial scanning is achieved by simply varying the drive voltage to E1. In addition, a new addition to the system design is added. Specifically, to compensate for aberrations, in particular spherical aberration introduced due to the presence and operation of E1 within a high NA objective, two (or more) additional E-lenses E2 and E3 with independent drive signals are used. Unlike [22, 24-27], here the E-lens used is a liquid lens which has the additional advantage of being polarization-insensitive and broadband as compared to a typical nematic liquid crystal lens. More importantly, the liquid

E-lens can form both positive and negative focus lenses via voltage control allowing the introduction of the required positive and/or negative focus wavefronts that can be used to reduce the spherical aberration in the scanned sample. Note that the use of E2 and E3 can also compensate from spherical aberrations that occur in the specimen when there is a refractive index mismatch between the specimen material and the index matching immersion fluid (and slide). Earlier, deformable mirror spatial light modulators with multiple electrical drive signals (for the many, e.g., 37 actuators in the mirror membrane) have been used to reduce aberrations in confocal microscopes [28]. In the Fig.1 design, only two electrical drive voltages are possibly needed to perform a similar function, hence reducing the complexity of the microscope. Experiments to be conducted later will give a better indication to the number of E-lenses needed for adequate aberration compensation.

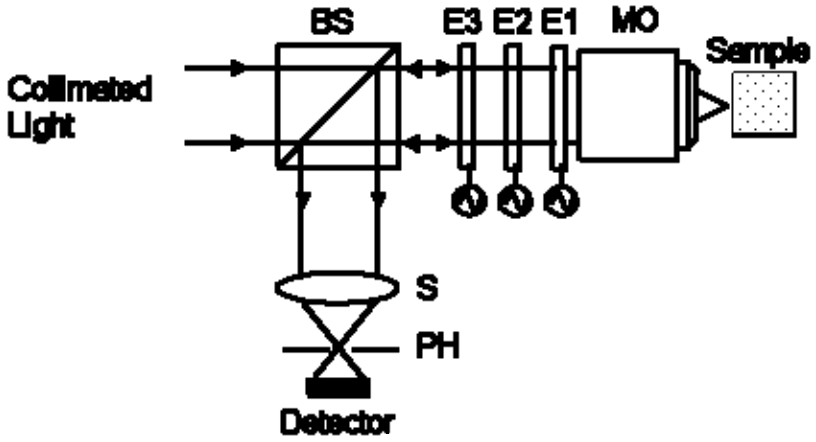

Fig.1. Proposed low aberrations Liquid lenses based confocal microscope design. BS: Beam-Splitter, MO: Micro-Objective, S: Spherical Lens, PH: Pinhole, E1, E2, E3: Liquid Lenses. E1: Axial Scanning Lens; E2 & E3: Aberration reduction E-lenses. S: Receiver Spherical Lens.

3. PROPOSED HIGH SPATIAL RESOLUTION SIGNAL PROCESSING METHOD

The goal is to implement 3-D imaging with higher resolution than possible with direct diffraction (and coherence) limited 3-D imaging. For example, in the case of a confocal microscope that is an excellent diffraction limited 3-D imager, the smallest size of an imaged volume element (also called voxel) is on the order of the EM-wave wavelength. For simplicity, one can assume a cartesian x,y,z coordinate system and the smallest size of the diffraction-limited symmetric voxel to be X by X by X microns (see Fig.1). Of course, in a practical scenario, all sides of the voxel may not exactly be the same. In fact, in confocal microscopy one can design the optical instrument such that the axial resolution (along optical beam direction) is two times smaller than the transverse diffraction limited (Abbe) resolution (e.g., via a 4-Pi Confocal Microscope). In effect, one can get sub-wavelength resolution with an optical confocal microscope, but not several orders of magnitude direct improvement in resolution over diffraction limits.

The steps for implementing the proposed high resolution 3-D processing are as follows (see Fig.2-6). Given the low resolution voxel of sides X (see Fig.2), first 1-D high resolution optical data is acquired along the three axial look directions of the voxel. For each axial look direction, the 1-D high resolution optical data is produced by using a known computer processing algorithm [11, 16-17]. In effect, for each axial look direction, the voxel is shifted (see Fig.3a,b,c)) in its axial direction by a given high resolution amount (e.g., X/2N) and 2N values of optical data are taken. No shift is implemented in the transverse direction of the voxel. This X/(2N)axial high resolution shift can be obtained by either moving the voxel (object under evaluation) using high resolution mechanics (e.g., Nano or Micro-mechanics; NEMS or MEMS stages) or by moving the focus position in the confocal microscope by a variable focal length electronic or mechanical/deformable weak lens (possible using liquid crystals, deformable mirrors, MEMS, NEMS, fluids, oils, electro-wetting techniques, etc), (e.g., in OCT, change the axial location of the reference mirror). As an example, if X= 1 micron, then with 2N=1000 steps, the axial motion step required is 1 nm. Such precision motion is possible with today's high resolution mechanics plus programmable liquid crystal or other no-moving parts lenses [22-24]. Another known approach for axial scanning is using a broadband optical source (or a tunable laser) with a dispersive lens [29-30]. In this case each wavelength can be designed to represents a standard of classic axial low resolution slice. One new proposed option is to use fine tuning of the source or detection filter to select finer wavelengths between each axial resolution

window to be able to move the axial focus of the confocal focus position on a nanometer or even Angstrom scale. This process because it is analog can lead to extremely fine high resolution axial shifts as required for the proposed data processing.

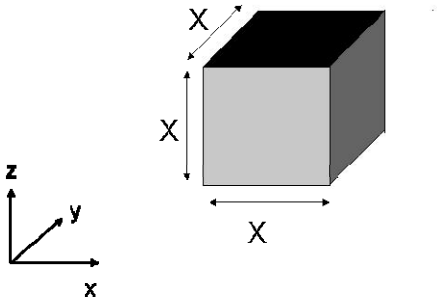

Fig. 2: Low resolution voxel obtained via traditional 3-D imaging methods. This voxel is to be imaged with high 3-D resolution.

Using the acquired 2N high resolution axial shift data values for a given axial direction, one applies the mentioned computer algorithm (e.g., IBP or MLE or IBD) to get the N high resolution axial slice data (each of size X/N) for the given look direction (see Fig.4). These computer algorithms require the use of the Point Spread Function (PSF) of the imager. The PSF can be measured experimentally, theoretically utilized from known classic expressions, or estimated via computer calculations. In this case, because of the proposed axial sectioning (not transverse direction shifting) for data collection, the PSF can be well estimated in most cases by the classic [Sinc function]4 function axial response (intensity distribution along the optical axis) of the confocal microscope that can also be optimized to be better than the transverse resolution response of the microscope. Fig.3 (a), (b), and (c) show the high resolution motion of the low resolution voxel in the x, y, and z axial directions, respectively. Do note that the figures also show shifted voxel in the non-axial directions, but this is only for clarity of diagrams. In practice, only axial motion of voxel is implemented to gather the optical irradiance data off the low resolution voxel element keeping the voxel stationary in the transverse optical coordinates.

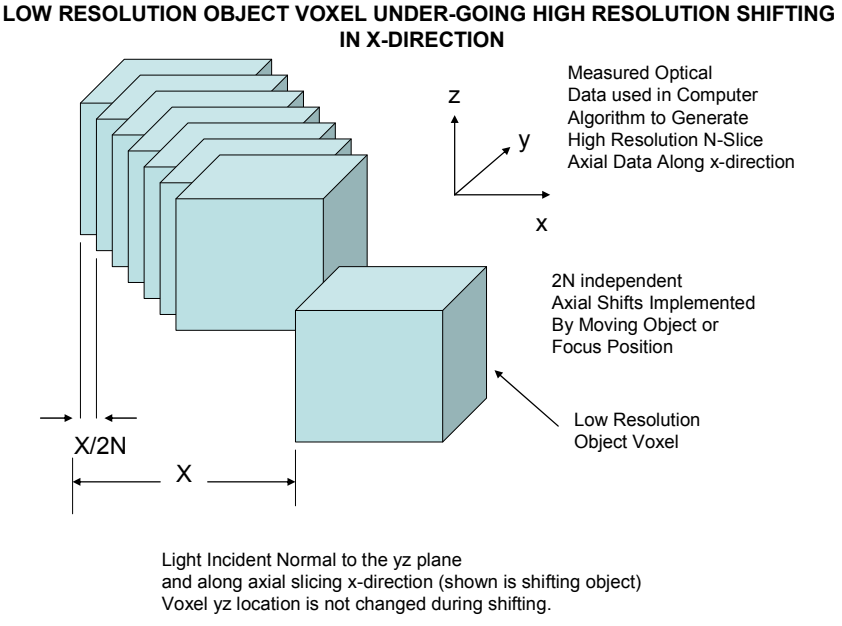

(a)

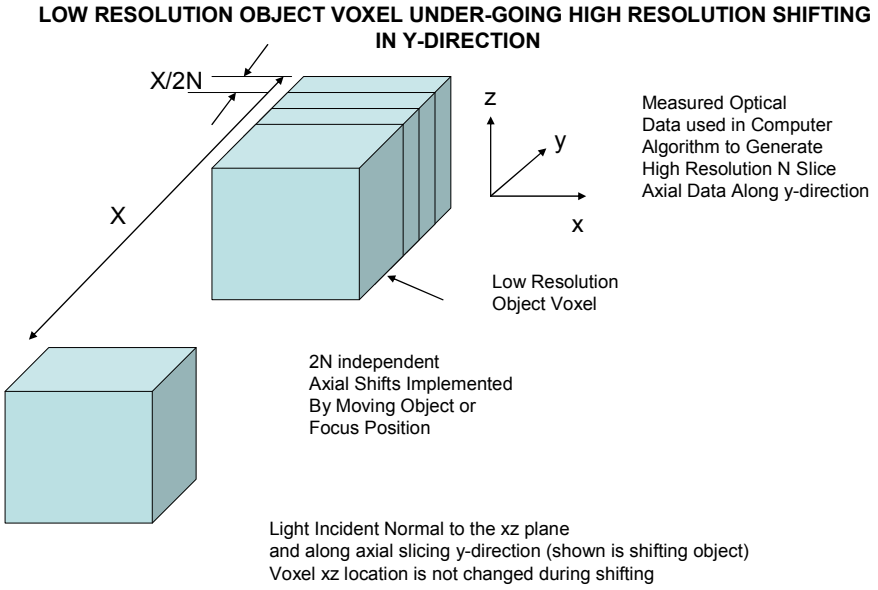

(b)

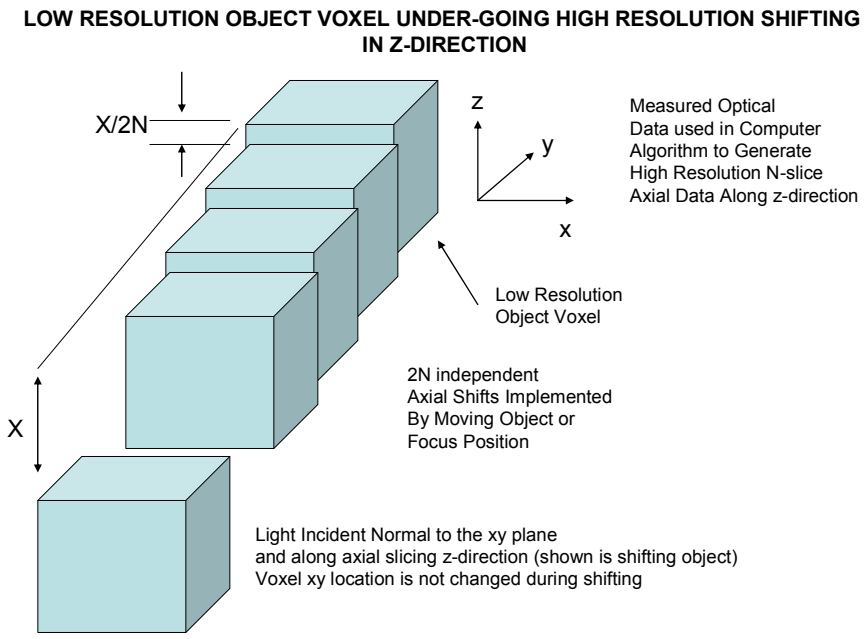

(c)

Fig.3. (a) The high resolution motion of the low resolution voxel in the x axial direction, (b) the high resolution motion of the low resolution voxel in the y axial direction, (c) the high resolution motion of the low resolution voxel in the z axial direction.

For the y axial look direction, after computer-based algorithm processing one gets N optical data values representing the voxel transverse (xz) irradiance values given as $I_{xz}(i_y)$ where i_y goes from 1 to N (see Fig.4a). Similarly, for the z axial look direction, after computer processing one gets N optical data values representing the voxel transverse (xy) irradiance values given as $I_{xy}(i_z)$ where i_z goes from 1 to N (see Fig.4b). Finally, for the x axial look direction, after computer processing one gets N optical data values representing the voxel transverse (yz) irradiance values given as $I_{yz}(i_x)$ where i_x goes from 1 to N (see Fig.4b).

High Resolution 1-D N-Slice Optical Irradiance Data along Y-Axial Direction Generated via Computer Algorithm using High Resolution Y-Direction 2N Axial Shifts of Low Resolution Voxel

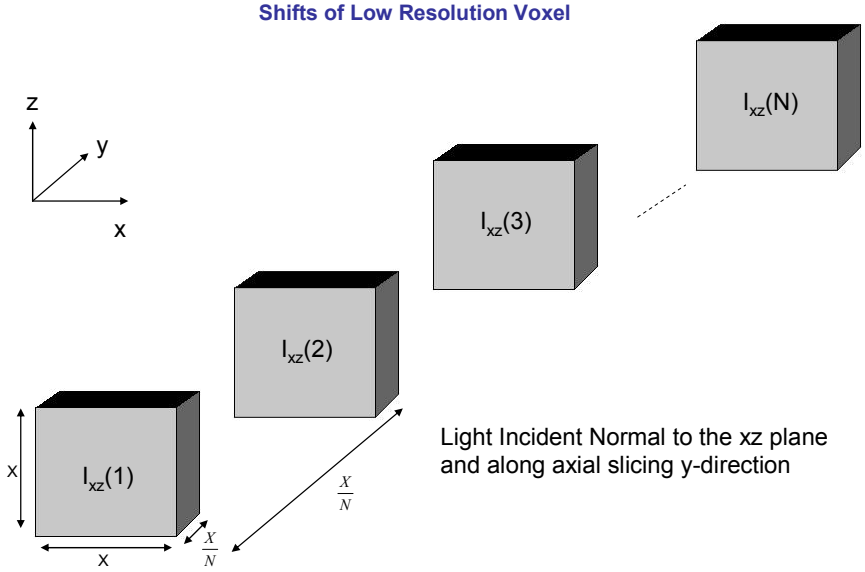

(a)

High Resolution 1-D Optical Irradiance N-Slice Data along Z-Axial Direction Generated via Computer Algorithm using High Resolution Z-Direction 2N Axial Shifts of Low Resolution Voxel

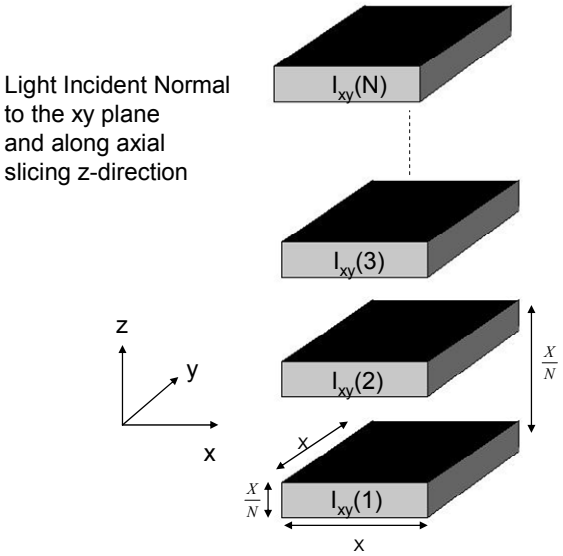

(b)

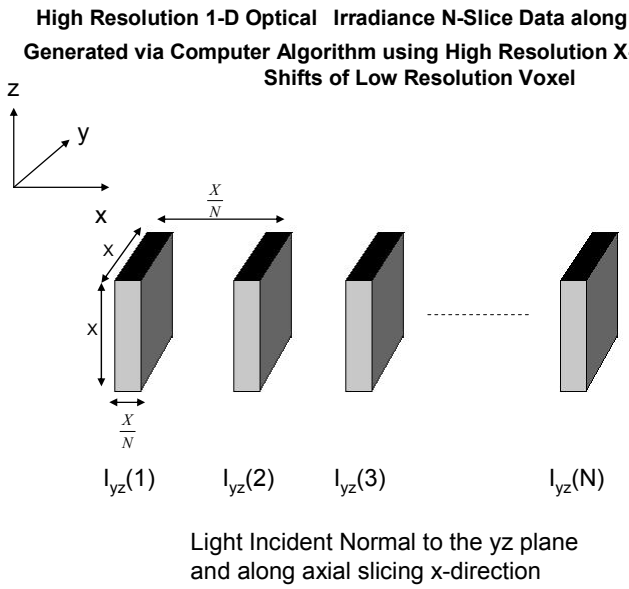

Fig.4 .(a) High Resolution 1-D Optical Irradiance Data along Y-Axial Direction Generated via Computer Algorithm using High Resolution Y-Direction Axial Shifts of Low Resolution Voxel, (b) High Resolution 1-D Optical Irradiance Data along z-Axial Direction Generated via Computer Algorithm using High Resolution z-Direction Axial Shifts of Low Resolution Voxel. (c) High Resolution 1-D Optical Irradiance Data along x-Axial Direction Generated via Computer Algorithm using High Resolution x-Direction Axial Shifts of Low Resolution Voxel.

Note the high resolution data is indeed Nyquist sampling limited in bandwidth to N/X as the sampling frequency is twice this bandwidth or 2N/X. The next step is to interpolate this Ixz(iy), Ixy(iz), Iyz(ix) data sets to realize a 3-D super resolution voxel such as shown in Fig.5 coordinate system with super resolution voxel sides of .(X/N) x M where the numbers N and M dictate the improvement in resolution. If M = 1, a maximum improvement in voxel resolution is achieved but at the cost of the largest reconstruction error. If M = N, there is no improvement in voxel resolution compared to the low resolution voxel of sides X and the reconstruction error is also zero. The value of M is set to a value between 1 and N so that the reconstruction error comes out to be at an acceptable value, e.g., < 10 %. Early simulations show that for N=200 and M=2, a 100 times better voxel resolution is achieved within a < 9% error from true high resolution voxel irradiance values. This case assumed a true one-to-one reconstruction of high resolution irradiance axial slices from the shifted low resolution voxel axial slice data via the computer algorithm data. In reality, the computer produced data will also have an error value.

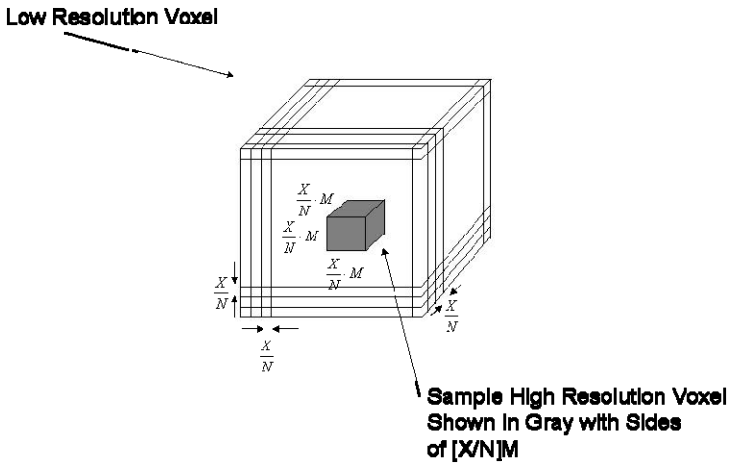

Fig.5. Shown is a typical high resolution voxel within the low resolution voxel of sides X.

Defined for any super resolution 3-D voxel is an irradiance weight $I_{xyz}(a,b,c)$ between 0 and 1, where a,b and c are the new super resolution coordinates each going from 1 to N/M. In this case,

$$I_{xyz}(a,b,c) = \frac{1}{3}\left(\sum_{i_x = M\cdot(a-1)+1}^{M\cdot(a-1)+M} I_{yz}(i_x) + \sum_{i_y = M\cdot(b-1)+1}^{M\cdot(b-1)+M} I_{xz}(i_y) + \sum_{i_z = M\cdot(c-1)+1}^{M\cdot(c-1)+M} I_{xy}(i_z) \right) \cdot \frac{M^2}{N^2} \qquad (1)$$

$$a,b,c \in [1,2,3,.....,N/M]$$

The limits on the summations show that only the slices that contain the super-resolution voxel are used in its reconstruction. Here it is assumed that the super resolved irradiance values [i.e., $I_{xz}(i_y)$, $I_{xy}(i_z)$, $I_{yz}(i_x)$] are isotropic radiators for any given material subject to the proposed 3-D imaging, a reasonable assumption considering the small scale of the super-voxel with respect to the radiation wavelength. Note that each 2-D Irradiance slice value [i.e., $I_{xz}(i_y)$, $I_{xy}(i_z)$, $I_{yz}(i_x)$] contains N/M new super pixels in one transverse direction and N/M new super pixels in the other transverse direction. For example, each $I_{xz}(i_y)$ values is produced over a transverse average of N/M super resolution pixels in the x-direction and N/M super resolution pixels in the z direction, while along the y-direction, it is a single super pixel. Hence, each summed irradiance value per transverse data set must be divided by $(N/M)^2$ to get the normalized super resolution voxel average. Since there are 3 transverse irradiance data sets [i.e., $I_{xz}(i_y)$, $I_{xy}(i_z)$, $I_{yz}(i_x)$], one must also divide the entire sum by 3, hence the required 3-D processing Eqn.1.

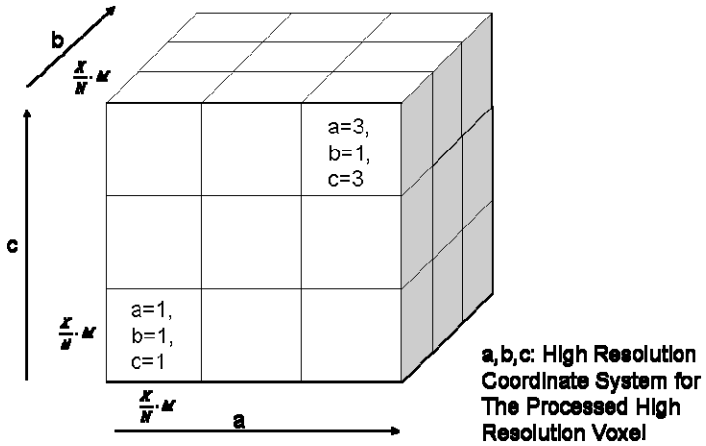

Fig.6. The (a,b,c) coordinate system for the reconstructed super-resolution voxel.

Recall that X was taken as the x,y,z direction spatial resolution limit of the EM wave due to diffraction, etc. Now the reconstructed super resolution 3-D voxel basic building block is of size (X/N)M. Therefore, using the proposed processing, a voxel imaging resolution improvement of E is achieved where E is given by:

$$E = \frac{X}{(X/N)\cdot M} = \frac{N}{M}. \qquad (2)$$

If X= 1micron, and 2N=1000 with axial shifts needed per 1 nm, the final voxel super resolution after the proposed innovation implementation is 2 nm per side, a 500 X improvement on the low resolution voxel of 1 micron sides. Note that the shifting operation of the low resolution axial scans is a form of signal sampling. Smaller the shift, higher the sampling frequency and hence higher the bandwidth of the recovered high resolution axial scan. Although a shift with X/(2N) steps leads to signal reconstruction with X/N resolution (the Nyquist limit), a better signal reconstruction can be achieved by over-sampling the original signal at much higher rates that the Nyquist rate. Thus, higher quality signal recovery is achieved at the cost of lowering the bandwidth of the recovered signal, e.g., resolution could be for example, (4X)/N instead of X/N for the Nyquist rate. Based on type of signal data that depends on various factors such as optical confocal microscope parameters and test sample optical properties, optimal sampling/shift rates/sizes can be picked to produce the best high resolution axial slice data. Here, pure analog motion of the confocal light focal point via an analog lens focal length control process (e.g., via liquid crystal, liquid, or MEMS device) is key as extremely tiny optical axial steps can be possible. Also, because confocal or on-axis shifting and data collection is involved on a point-only basis in a

given sample transverse plane, no traditional image noise is present as data is collected on a single transverse resolution basis in the proposed signal processing method. Hence, improved high resolution 3-D signal reconstruction is expected.

4. SIGNAL PROCESSING COMPUTER SIMULATIONS

To prove the concept of the aforementioned signal processing approach, a computer simulation is carried out. Fig. 7 shows a random high resolution 1-D signal generated using a computer that has 2N = 2000 resolution bins along the axial direction. Fig. 8 shows an example theoretical PSF for a confocal microscope having a resolution of 100 units. The Fig. 7 high resolution signal is sampled using the Fig. 8 PSF at 2 unit shifts to generate 1000 experimental low-resolution signals in the same way to what would be acquired using a confocal microscope. Each low resolution signal has 20 resolution bins along the axial direction as they are generated using a PSF that is 100 units wide.

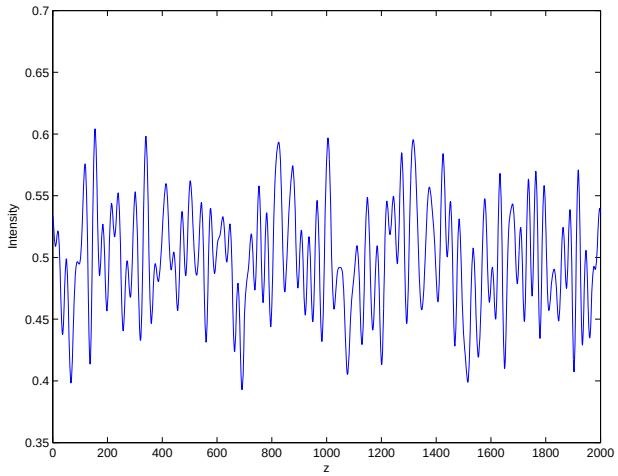

Fig. 7. Original computer generated random 1-D high-resolution axial scan signal.

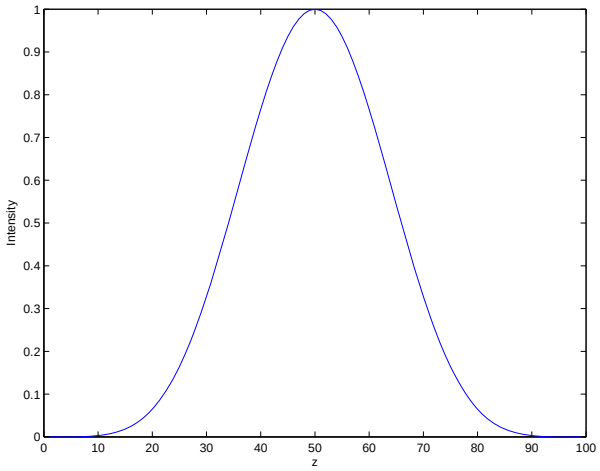

Fig. 8. Classic theoretical confocal Point Spread Function (PSF).

Once the low-resolution signals are acquired, Iterative Back Projection (IBP) algorithm [11] is used to reconstruct a high-resolution signal. The algorithm operates by first making a guess to the high-resolution signal and then sampling the guess using the PSF to generate low-resolution signals. These guessed low-resolution signals are then compared to the experimental low-resolution signals and depending on the error, the guess for the high resolution signal is updated. This process is iteratively repeated until the difference between the reconstructed low resolution signals and the experimental low-resolution signals is below a certain threshold. Figs. 9 (a), (b) and (c) show these reconstructed signals at different iterations of the algorithm. Fig. 10 shows the final reconstructed high resolution signal super-imposed on top of the original high resolution signal. The difference between the two signals is plotted in Fig. 11 showing that the mean-

square error between the original and the reconstructed signals is an extremely small 2.5476 x 10-4 for a resolution improvement by a factor of 50.

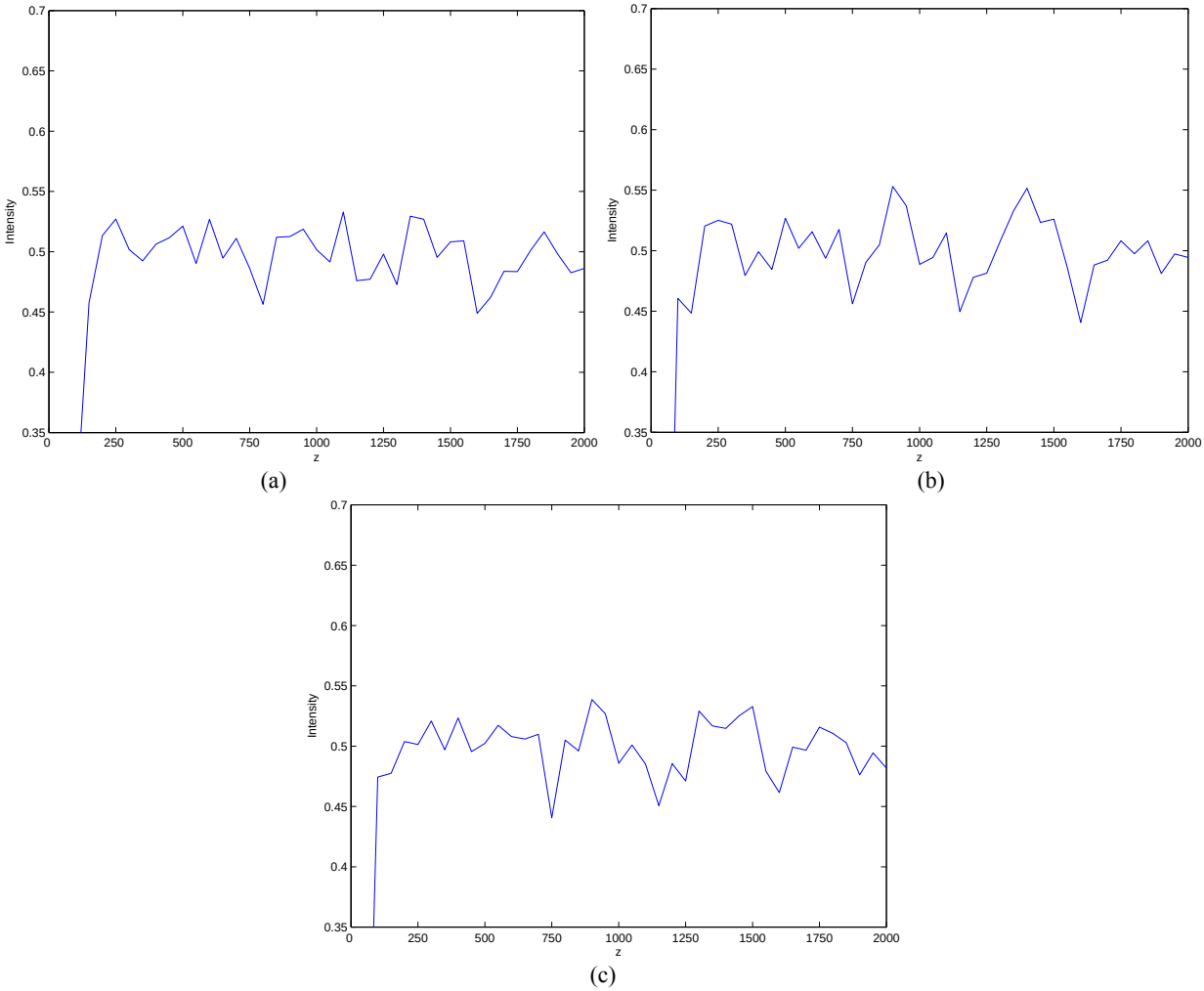

Fig. 9. Reconstructed low-resolution signals at different stages of iteration.

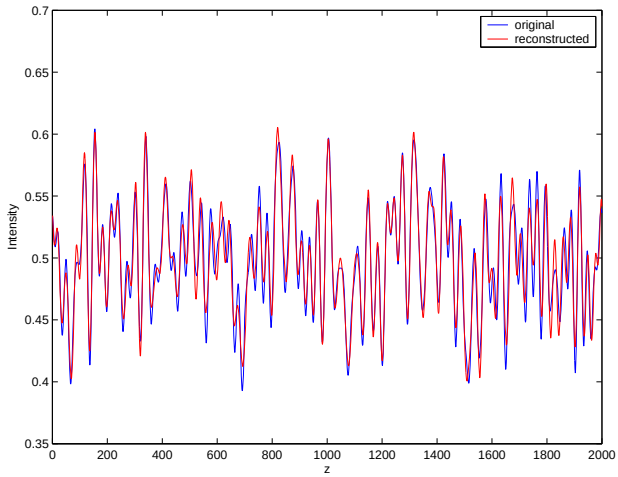

Fig. 10. Reconstructed higher resolution axial signal.

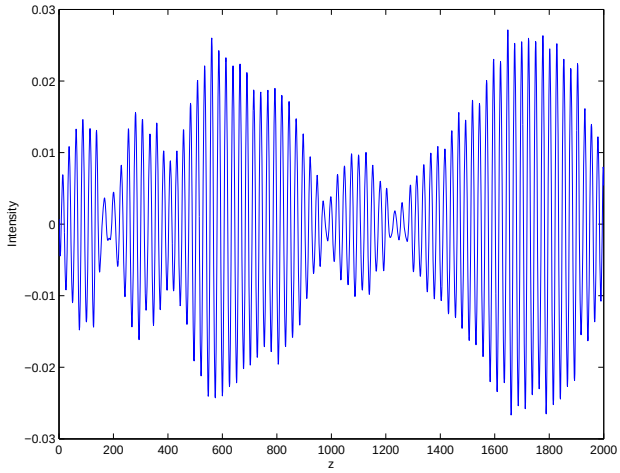

Fig. 11. Mean square error between the original and the reconstructed high resolution signals.

Next, for a computer-generated random 3-D signal, for each of the three look directions, a similar process is carried out to generate 1-D high resolution signals. These are then combined using Eq. 1 to generate a 3-D super-resolution signal. Depending on the factor of resolution improvement E chosen, different amounts of error would be observed between the original and the reconstructed 3-D signals. The mean of absolute differences between the two are plotted as a function of E is Fig. 12. The Fig. 12 data shows that for a resolution improvement factor of E=50, the reconstruction error is only 4.4% while for a resolution improvement factor E = 100, the reconstruction error is 8.8%.

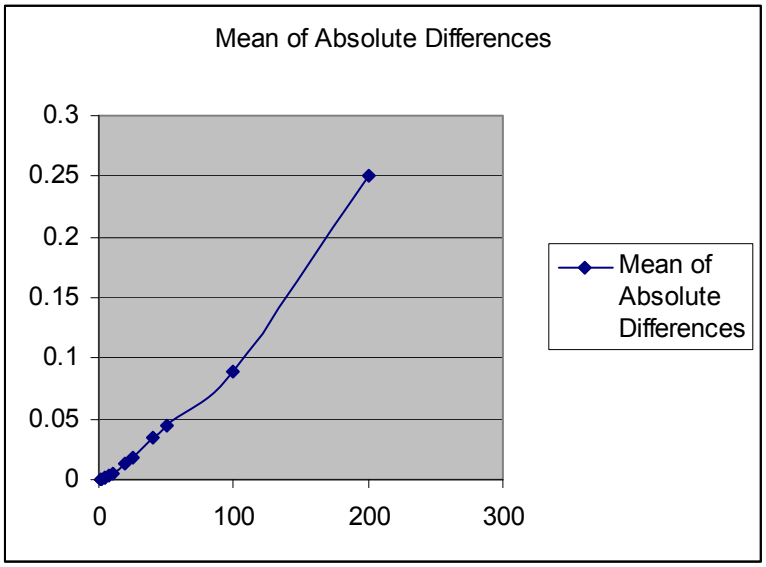

Fig. 12. Mean Absolute Difference versus resolution improvement factor, E.

5. CONCLUSION

For the first time, proposed is a minimal-moving-parts low aberrations axial scan confocal microscope design using liquid lens technology. It is further proposed how a diffraction-limited confocal microscope can be used to give higher resolution images using advanced signal processing methods. The proposed E-lens based microscope is especially suitable for non-contact ophthalmological imaging applications e.g. cornea and eye lens imaging. Future work would focus on experimental demonstration of these new ideas.

6. ACKNOWLEDGEMENTS

The authors would like to thank Dr. Frank Perez (Nuonics) and Dr. Florian Bociort (TU Delft) for their technical insights. Prof. N. A. Riza acknowledges the EU 2008 Eramus Mundus Opt-Sci Program for his visiting Professorship at TU-Delft, The Netherlands.

7. REFERENCES

1. M. Gustafsson, ”Surpassing the lateral resolution limit by a factor of two using structured illumination microscopy,” J. Microscopy, Vol. 198, pp. 82-87, May 2000;
2. X. Huang and J. Tan, ” A new super-resolution element for array confocal microscopy,” Meas. Sci. Tech, Vol. 17, pp. 601-604, 2006;
3. W. Zhao, J. Tan and L. Qiu ., “Bipolar absolute differential confocal approach to higher spatial resolution,” Opt. Express, Vol. 12, pp. 5013-5021, 2004.
4. S. Hell & E. Stelzer, "Properties of a 4Pi confocal fluorescence microscope," J. Opt. Soc. Am. A, Vol. 9, pp. 2159-2166, 1992
5. M. Gustafsson, Agard and Sedat,” I^5M: 3D widefield light microscopy with better than 100 nm axial resolution,” J. Microscopy, Vol. 195, pp. 10-16, July 1999;
6. O. Haeberle, B. Simon, “Improving the lateral resolution in confocal fluorescence microscopy using laterally interfering excitation beams,” Optics Comm., Vol. 259, pp. 400-408, 2006;
7. TA Klar, S Jakobs, M Dyba, A Egner, SW Hell, “Fluorescence microscopy with diffraction resolution barrier broken by stimulated emission,” PNAS, Vol. 97, pp. 8206-8210, July 18, 2000;
8. M. Dyba & S. Hell, “Focal Spots of Size λ/23 Open Up Far-Field Florescence Microscopy at 33 nm Axial Resolution,” Phys. Rev. Lett., Vol. 88, pp. 163901, 22 April 2002;
9. E. Stelzer, “Light microscopy: Beyond the diffraction limit?,” Nature, Vol. 417, pp. 806, June 2002.
10. Confocal and Two Photon Microscopy, Ed. A. Diaspro, Chapter 12: Image Restoration Methods, P. Boccacci and M. Bertero, Wiley, 2002.
11. M. Irani and S. Peleg, “Motion analysis for *image* enhancement:. resolution, occlusion and transparency,” J. Vis. Comm. Image Rep., Vol. 4, pp. 324-335, 1993.
12. Y. Lu and M. Inamura, “Spatial resolution improvement of remote sensing images by fusion of subpixel-shifted multi-observation images,” Int. J. Remote Sensing, Vol. 24, pp. 4647-4660, 10 Dec. 2003.
13. S. Peled and Yehezkel Yeshurun, ”Superresolution in MRI: Application to human white matter fiber tract visualization by diffusion tensor imaging,” Proc. Int. Magnetic Reson. Med.9, 2001.
14. W. Carrington, R. Lynch, E. Moore, G. Isenberg, K. Fogarty, “Superresolution three-dimensional images of fluorescence in cells with minimal light exposure,” Science, Vol. 268, pp. 1483, June 1995.
15. M. Schrader, S. Hell, H. Van der Voort, “Three-dimensional super-resolution with a 4Pi-confocal microscope using image restoration,” J. Appl. Phys., Vol. 84, pp. 4033-4042, 1998.
16. T. J. Holmes, “Expectation-maximization restoration of band-limited, truncated point-process intensities with application in microscopy,” J. Optical Soc. America A, Vol. 6, pp. 1006-1014, 1989.
17. T. J. Holmes, “Blind deconvolution of quantum-limited incoherent imagery: maximum-likelihood approach,” J. Optical Soc. America A, Vol. 9, pp. 1052-1061, 7, July 1992.
18. G. Westheimer and S McKee, “Spatial Configurations for Visual Hyperacuity,” Vision Research, Vol. 17, pp. 941-947, 1977
19. P. Baldi and W. Heiligenberg, “How Sensory Maps Could Enhance Resolution Through Ordered Arrangements of Broadly Tuned Receivers,” Biol. Cybern, Vol. 59, pp. 313-318, 1988.
20. J. Zhang and J. Miller, “A mathematical model for resolution enhancement in layered sensory systems,” Biol. Cybern., Vol. 64, pp. 357-364, 1991.
21. F. Perez, “Hue Segmentation, Color Circuitry, and the Mantis Shrimp,” Ph.D. Thesis, California Institute of Technology, 1995.
22. N. A. Riza and A. Bokhari, “Agile Optical Confocal Microscopy Instrument Architectures For High Flexibility Imaging,” in Three Dimensional Confocal Microscopies, BIOS 2004 Biomedical Optics, Photonics West, Proc. SPIE Vol. 5324, Paper No. 14, pp. 77-88, San Jose, CA, January 2004.
23. N. A. Riza and S. A. Khan, “Polarization multiplexed optical scanner,” Opt. Lett., Vol.28, pp.561-563, 2003.

24. S. A. Khan and N. A. Riza, "Demonstration of a No-Moving-Parts Axial Scanning Confocal Microscope Using Liquid Crystal Optics," Opt. Comm., Vol. 265, pp. 461-467, 2006.
25. N. A. Riza, M. Sheikh, G. Webb-Wood, and P. Kik, "Demonstration of Three Dimensional Imaging of Blood Vessel using a No-Moving Parts Electronic Lens-based Optical Confocal Microscope," Conference MI03: Physics of Medical Imaging, SPIE Medical Imaging, Proc. SPIE Vol. 6510, pp. 65100J1-5, San Diego, CA, Feb. 2007.
26. Mumtaz Sheikh, Nabeel A. Riza, "Blood vessel 3-D imaging using electronically controlled optics lens-based confocal microscopy," in OSA BIOMED, St. Petersburg, FL, March 2008.
27. Nabeel A. Riza, Mumtaz Sheikh, Grady Webb-Wood, Pieter Kik, "Demonstration of three-dimensional optical imaging using a confocal microscope based on a liquid-crystal electronic lens," Opt. Eng. Vol. 47, pp. 063201 (2008).
28. L. Sherman, J. Y. Ye, O. Albert, and T. B. Norris, "Adaptive correction of depth-induced aberrations in multiphoton scanning microscopy using a deformable mirror," Journal of Microscopy**,** Wiley Press, Vol. 206, Issue 1, pp. 65 – 71, April 2002.
29. H. J. Tiziani & H. M. Uhde, "Three dimensional image sensing by chromatic confocal microscopy," Appl. Opt., Vol. 33, No. 10, pp. 1838-1843, 1994.
30. B. Picard, "Method for the scanning confocal light optical microscopic & indepth examination of an Extended field & devices for implementing said method," US Patent 4965441, Oct.23, 1990.